MATHEMATICAL MODEL FOR THE DYNAMICS OF AN ARTICULATED STRING OF FUEL BUNDLES IN AXIAL FLOW

M.P. PAÏDOUSSIS

Department of Mechanical Engineering, McGill University, Montréal, Québec, H3C 3G1, Canada

SUMMARY

This paper describes an analytical model for the dynamics of an articulated string of fuel bundles in axial flow, each bundle being composed of many fuel elements held between end plates, and the bundles being held together by a central support tube running through the whole assembly—as, for example, in the CANDU-BLW design.

The model is developed on the basis of Lagrangian formulation, in which the inter-bundle stiffnesses, the bundle shear stiffnesses and gravity forces are incorporated into the potential energy of the system, the conservative part of the inviscid hydrodynamic forces are incorporated into the kinetic energy, and the nonconservative part, as well as viscous forces and pressure forces, are incorporated into the generalized forces of the system. The model is one-dimensional. For a system of N bundles, one has 2N generalized coordinates representing the total and the shear angular deflections.

The equations of motion were obtained in two ways: (a) by direct matrix manipulation of the Lagrangian equations, and (b) by an algebraic computer processor called FORMAC. The two methods yield identical results. In either case the end result is a matrix dynamical equation, where the dissipation and stiffness matrices are asymmetric.

A computer program has been developed which yields the eigenfrequencies and eigenvectors of the system, specified by the following input parameters: coefficients of friction in the lateral and axial directions; length, diameter and mass of each bundle; virtual mass of each bundle; hydraulic diameter of the bundle in the flow tube; mean density of the fluid at the centre-point of each bundle and the corresponding mean flow velocity; stiffnesses of the central support tube and the end plates, and shear stiffness of each bundle (which also specify how the ends of the fuel string are supported); hydrodynamic parameters associated with a free end; and direction of gravity.

Calculations were conducted for vertical systems with four and with twelve bundles, pinned at the bottom and free at the top, with the flow upwards.

The eigenfrequencies are generally complex; if the imaginary part is negative, the system is unstable, either by buckling or by flutter. Both types of instabilities were encountered for different sets of input parameters; buckling is sometimes due to gravity and sometimes is flow-induced. The eigenvectors are generally complex also, which indicates that free motions of the fuel string are not stationary; i.e. there are also wave-like motions involved; (such motions were observed in experiments with fuel strings in flow by Hancox and Forrest at Westinghouse Canada Ltd.)

For a given system, instabilities may be eliminated by making the string stiffer (e.g. increasing the tension of the central support tube and augmenting the end-plate stiffnesses), and proper design of the shape of the free end. Calculations show that careful design, may not only eliminate flow-induced instabilities, but may produce flow-induced damping which is useful in reducing vibration due to flow and pressure perturbations.

1. Introduction

An important consideration in the structural design of nuclear fuel assemblies is that they be free of hydroelastic instabilities and not subject to excessive flow-induced vibration. Thus, knowledge of the free-vibration characteristics (in flow) is a first and essential element in the proper design of fuel assemblies.

Until now, theoretical work was mainly directed at the dynamical analysis of individual fuel elements in flow (*vide* [1]). However, in many designs, fuel elements are assembled in bundles, and bundles are held together one on top of the other, forming so-called "fuel strings" which are capable of moving as cohesive structures. As the effective flexural rigidity of such fuel strings may be much inferior to that of individual fuel elements, it is reasonable to ask whether flow-induced motions of the fuel string as a whole are not as important, or perhaps more so, than motions of individual fuel elements. Indeed, damage to the pressure tube may be more likely from excessive vibration of the fuel string than of individual fuel elements.

This paper develops an elementary mathematical model for the dynamics of fuel strings in axial flow, capable of yielding the free vibration characteristics of the system. Although the model, as formulated, may be applied to any such system, it will be simpler to develop it in terms of a specific configuration, namely that of the CANDU-BLW reactor; the fuel bundles are compressed together by a central support tube (CST, for short), the fuel string is mounted vertically within a pressure tube, and is held at the bottom and free at the top, the flow being upwards.

The mathematical formulation will be given first (§2), followed by the derivation of the equations of motion (§3) and their solution (§4), and then by typical results and their interpretation (§5).

2. Mathematical formulation

The mathematical model assumes that the fuel string behaves like an articulated structure, with bundles as its elements. Lateral movements of the fuel string are considered to involve parallelogramming (shear) deformation of each bundle, as well as bending of the end-plates and the CST. During deformation, elements in each bundle are assumed to move parallel to one another.

The problem is analysed by Lagrange's method, with generalized coordinates ϕ_i the total angles of deflection, and ψ_i the angles due to bending alone (Fig. 1), where i=1,2,...N, the number of bundles being N. Other components of the fuel string, at the top and bottom of the string, which are not real bundles, will be treated as degenerate bundles to preserve the unity of the formulation.

2.1 The Structural model

Denoting the stiffnesses to shear, bending of the CST and of the end plates by c_i, k_i^*, k_i, respectively, and the mass of each bundle per unit

length by m_p, the potential energy of the structure is found to be

$$V = -\frac{1}{2}\sum_{p=1}^{N}\{\int_0^{\ell_p} m_p g[\sum_{q=0}^{p-1}\ell_q\phi_q^2 + \xi\phi_p^2]d\xi\} + \frac{1}{2}\sum_{p=1}^{N} c_p(\phi_p-\psi_p)^2$$

$$+\frac{1}{2}\sum_{p=1}^{N} k_{p-1}(\psi_p-\psi_{p-1})^2 + \frac{1}{2}\sum_{p=1}^{N} k_p^*(\phi_{p+1}-\phi_p)^2 \quad . \tag{1}$$

The kinetic energy is found to be

$$T_s = \frac{1}{2}\sum_{p=1}^{N}\{\int_0^{\ell_p} m_p[\sum_{q=0}^{p-1}\ell_q\dot{\phi}_q + \xi\dot{\phi}_p]^2 d\xi\} \quad . \tag{2}$$

2.2 Hydrodynamic forces

The fluid properties, e.g. the flow velocity and density, are assumed to vary along the length of the string as a result of heat generation; however, they will be considered to be approximately piece-wise linear along each bundle. Thus, the density at the mid-point of the pth bundle is represented by ρ_p, and the density at other points in the bundle by $\rho_p=\rho_p+\rho_p'(\xi-\frac{1}{2}\ell_p)$, $0<\xi<\ell_p$. The fluid properties at each cross-section are considered to be constant as a necessary simplifying assumption.

The fuel string is subject to inviscid and viscous hydrodynamic forces and to pressure forces. The conservative part of the inviscid hydrodynamic forces may be expressed as a kinetic energy

$$T_f = \frac{1}{2}\sum_{p=1}^{N}\{\int_0^{\ell_p} M_p[\sum_{q=0}^{p-1}\ell_q\dot{\phi}_q + \xi\dot{\phi}_p + U_p\phi_p]^2 d\xi\} \quad , \tag{3}$$

where M_p is the virtual mass of the pth bundle per unit length, and U_p is the flow velocity at the mid-point of the pth bundle. There is also a non-conservative force at the free end associated with the inviscid hydrodynamic forces,

$$F_{nc} = -(1-f)M_L U_L[\sum_{p=1}^{N}\ell_p\dot{\phi}_p + U_L\phi_N] \quad , \tag{4}$$

where $f\to 1$ for a streamlined free end, while $f\to 0$ for a square end.

The frictional forces per unit length acting on the pth bundle may be found [2] to be

$$\left.\begin{aligned}(F_L)_p &= \tfrac{1}{2}n\rho_p DU_p^2 C_f \quad ,\\ (F_N)_p &= \tfrac{1}{2}n\rho_p DU_p C_f[\sum_{q=0}^{p-1}\ell_q\dot{\phi}_q + \xi\dot{\phi}_p + U_p\phi_p]\\ &\quad + \tfrac{1}{2}n\rho DC_D[\sum_{q=0}^{p-1}\ell_q\dot{\phi}_q + \xi\dot{\phi}_p] \quad ,\end{aligned}\right\} \tag{5}$$

where $(F_L)_p$ is along the bundle and $(F_N)_p$ is normal to it; n is the number of elements in the bundle, each of diameter D.

Similarly, the pressure forces per unit length on the pth bundle are found to be

$$\left[F_{P_y}\right]_p = -\left[\tfrac{1}{2}n\rho_p DU_p^2 C_f \frac{D}{D_h} + \rho_p g A_p + \rho_p A_p U_p \left(\frac{\partial U}{\partial x}\right)_p\right]\phi_p \ . \qquad (6)$$

Finally, there is a base drag at the free end which may be represented by $\frac{1}{2}\rho_L D_{eq} U_L^2 C_b$, D_{eq} being an equivalent diameter of the free end and C_b being a base drag coefficient.

To derive these expressions it was necessary to make a number of drastic simplifications in the interest of making the model tractable.

3. The equations of motion

The sum of eq. (2) and (3) is the total kinetic energy, while eq. (1) is the potential energy. By considering the virtual work generated by the rest of the forces, one obtains the generalized forces. Hence, in principle, by application of Lagrange's equation, one may obtain the 2N equations of motion. However, the task is not simple, particularly for large N, and methods other than by hand manipulation were sought.

Two methods were utilized, both leading to the matrix equation

$$[M]\left\{\begin{matrix}\ddot{\phi}\\ \ddot{\psi}\end{matrix}\right\} + [C]\left\{\begin{matrix}\dot{\phi}\\ \dot{\psi}\end{matrix}\right\} + [K]\left\{\begin{matrix}\phi\\ \psi\end{matrix}\right\} = \{0\}. \qquad (7)$$

The first method utilized FORMAC programming, a computer system capable of doing algebraic (symbolic), as opposed to numerical, manipulations [3]; thus, it may perform operations such as $A=(x+y)^2 + 2xy$ and print $A=x^2+y^2+4xy$, or $(d/dx)x^3=3x^2$. The program performed all the necessary algebra, integrations and differentiations, and the sorting and collecting of terms, finally generating a set of punched cards giving expressions for the elements of [M],[C] and [K]. Part of the printed output for a case of N=12 is given in Fig. 2; TH(2,2,1) is the coefficient of $\dot{\phi}_2$ in the second equation of motion, i.e. it is the element C_{22} of [C].

The second method made use of matrix operator calculus, defining the requisite operators which extract directly from the kinetic and potential energies and from the generalized forces the matrices [M], [C] and [K].

As an example, let us consider the kinetic energy of the structure, T_s, which may be written as

$$T_s = \frac{1}{2}\sum_{p=1}^{N} m_p \ell_p \left[\left(\sum_{q=0}^{p-1} \ell_q \dot{\phi}_q + \tfrac{1}{2}\ell_p \dot{\phi}_p\right)^2 + \frac{1}{12}\ell_p^2 \dot{\phi}_p^2\right], \qquad (8)$$

and in matrix form as

$$T_s = \tfrac{1}{2}\{\dot{\phi}\}^T [\alpha]^T \left([m]*[\ell]\right)^D [\alpha]\{\dot{\phi}\} + \tfrac{1}{2}\{\dot{\phi}\}^T \left(\frac{1}{12}*[m]*[\ell^3]\right)^D \{\dot{\phi}\},$$

where superscript T denotes the transpose, superscript D denotes a diagonalized matrix, and $[\alpha] = ([\Omega] + \frac{1}{2}[I])[\ell]^D$, where $[\Omega]$ is a square matrix with elements equal to unity below the diagonal and zero elsewhere, and [I] is the

unit matrix, so that for N=2 we have

$$[\alpha] = \left(\begin{bmatrix} 0 & 0 \\ 1 & 0 \end{bmatrix} + \begin{bmatrix} \frac{1}{2} & 0 \\ 0 & \frac{1}{2} \end{bmatrix}\right)\begin{bmatrix} \ell_1 & 0 \\ 0 & \ell_2 \end{bmatrix} = \begin{bmatrix} \frac{1}{2}\ell_1 & 0 \\ \ell_1 & \frac{1}{2}\ell_2 \end{bmatrix}$$

Clearly, the contribution to the mass matrix due to T_s, e.g. for N=2 is

$$\begin{aligned}[M]_s &= [\alpha]^T([m]*[\ell])^D[\alpha] + \left(\frac{1}{12}*[m]*[\ell^3]\right)^D \\ &= \begin{bmatrix} \frac{1}{2}\ell_1 & \ell_1 \\ 0 & \frac{1}{2}\ell_2 \end{bmatrix}\begin{bmatrix} m_1\ell_1 & 0 \\ 0 & m_2\ell_2 \end{bmatrix}\begin{bmatrix} \frac{1}{2}\ell_1 & 0 \\ \ell_1 & \frac{1}{2}\ell_2 \end{bmatrix} + \frac{1}{12}\begin{bmatrix} m_1\ell_1^3 & 0 \\ 0 & m_2\ell_2^3 \end{bmatrix} \\ &= \begin{bmatrix} \frac{1}{3}m_1\ell_1^3 + m\,\ell_1^2\ell_2 & \frac{1}{2}m_2\ell_1\ell_2^2 \\ \frac{1}{2}m_2\ell_1\ell_2^2 & \frac{1}{3}m_2\ell_2^3 \end{bmatrix},\end{aligned}$$

which checks with what may be obtained directly from eq. (2) or eq. (8).

4. Solution of the equations

If one considers solutions of the form

$$\begin{Bmatrix} \phi \\ \psi \end{Bmatrix} = \begin{Bmatrix} \Phi \\ \Psi \end{Bmatrix} e^{i\omega t} \qquad (9)$$

then, for non-trivial solution, eq. (7) leads to a vanishing determinant

$$|-\omega^2[M] + i\omega[C] + [K]| = 0. \qquad (10)$$

This equation may be solved to find the 2N eigenfrequencies and the corresponding eigenvectors of the system.

Alternatively, the system may be transformed to one of first order involving a state vector $\{y\} = \{\dot{\phi},\dot{\psi},\phi,\psi\}^T$, which may be solved as a standard eigenvalue problem, yielding 4N eigenfrequencies and eigenvectors. Excepting purely imaginary frequencies, the frequencies appear in complex conjugate pairs of $i\omega$; and those with a negative real part are not physically meaningful.

5. Free vibration characteristics

5.1 General character of free motions

It is noted that, whereas [M] is symmetric, [C] and [K] are not, as a result of the hydrodynamic terms in these latter matrices.

The eigenfrequencies of the system at zero flow velocity are wholly real in the absence of dissipative forces, [C] being null. The corresponding eigenvectors, [K] now being symmetric, are orthogonal. If the fuel string is sufficiently long, because the weight of the fuel far outweighs the buoyancy force, buckling in the first and higher modes may result; the eigenfrequencies associated with modes in which buckling occurs are wholly imaginary.

With flow, the eigenfrequencies generally become complex; if the imaginary part of a frequency is positive, $\mathrm{Im}(\omega_i)>0$, while the real part, $\mathrm{Re}(\omega_i)\neq 0$, this indicates that the system is damped in that mode; if, however, $\mathrm{Im}(\omega_i)<0$ and $\mathrm{Re}(\omega_i)\neq 0$, this indicates the existence of flutter in that mode. The

eigenvectors with flow become similarly complex, and since [C] and [K] are now non-symmetric and the system non-Hermitian, the eigenvectors are also non-orthogonal. Since the eigenvectors are complex, this indicates that normal modes no longer exist, and the mode shapes are no longer stationary; i.e. there are travelling wave components in the free motions of the system. Some experiments at Westinghouse Canada Ltd. using fuel strings in water flow [4] measured vibration cross-correlation spectral densities at different axial positions along the fuel string; maxima for non-zero time delays proved the existence of travelling wave components in the motions of the string.

Some theoretical mode shapes, of the second and fifth modes, for a system of twelve bundles (N=12) when flow is present are shown in Fig. 3. Two aspects are immediately obvious; (a) the modes are not stationary, and (b) the mode shapes in flow differ from those at zero flow. The latter point is most evident in the case of the second mode, where we note the presence of a third-mode zero-flow component. This trend continues with increasing flow, and eventually the second mode in flow may look like the third mode at zero flow - with similar changes in other modes.

At small flow velocities, all eigenfrequencies have $\mathrm{Im}(\omega_i)>0$, indicating that flow damps free motions, except for the modes in which the system is buckled. With increasing flow, buckling disappears; this is intuitively obvious, since drag forces tend to "lift" and straighten the fuel string.

Increasing flow further, hydroelastic instabilities become possible. Flow no longer damps free motions in some modes and some $\mathrm{Im}(\omega_i)$ become negative, indicating either flutter or flow-induced buckling. Generally, these instabilities are possible when the dimensionless flow velocity $u = (MLN/k^*)^{\frac{1}{2}}U$ or $(MLN/c)^{\frac{1}{2}}U$ become greater than unity, where M is a typical virtual mass of a bundle per unit length, k^* and c are typical stiffnesses, L is the total length of the fuel string, N is the number of bundles per string, and U a typical value of flow velocity.

5.2 Illustrative calculations

Most of the above may be illustrated by calculations for four-bundle strings (N=4). Fig. 4 shows the eigenfrequencies plotted as an Argand diagram with flow velocity, U, as the parameter, for an arbitrary system with $\ell_1=\frac{1}{2}\ell_2=\ell_3=2\ell_4=1$, $m_1=2m_2=m_3=2m_4=10$, $M_i=4$, $U_i=U$, $k_1^*=0$, $k_2^*=k_3^*=1.5\times10^3$, $k_0=750$, $k_1=0$, $k_2=k_3=k_4=10^6$, $c_1=10^6$, $c_2=c_3=c_4=2.5\times10^3$, $\rho_i=750$, $A_i=5.79\times10^{-3}$, $D_i=1.97\times10^{-2}$, $D_i/D_h=3.28$, $C_f=3.3\times10^{-3}$, g=9.81, n=19, $D_{eq}=6\times10^{-2}$, $C_b=0.2$ and f=0.8 in consistent units. It is seen that the system is buckled in its first mode at U=0; it briefly regains stability at U=18 when $\mathrm{Im}(\omega)\simeq0$ for the negative branch of the first mode (1- mode), but flow-induced buckling sets in until U=54. This coincides approximately to the flow velocity where the system loses stability by flutter, first in its second mode and then in its third mode.

Thus, hydroelastic buckling is the dominant instability in this case. The first-mode locus is also shown in Fig. 5 plotted as a function of U.

Also shown is the first mode of an otherwise identical system, but with f=0.5, i.e. a blunter free end. The effect is very significant. Buckling disappears at U≃6. At point A of Fig. 5, the positive and negative branches of the first mode coalesce and leave the Im(ω)-axis and thence the system remains stable to at least U=45.

Fig. 6 shows the eigenfrequencies of the same system as in Fig. 4, but with the bundle lengths doubled, and all stiffnesses ten times smaller. In this case at zero flow the system is buckled in both first and second modes. With increasing flow it regains stability in its second mode at U≃4, and in its first mode at U≃5. However, subsequently, flow-induced buckling occurs at U≃12 which persists to at least U=20. Moreover, flutter occurs in the second mode for 15<U<18, approximately.

These calculations show that a string with a blunt end and high effective stiffness is the more likely to resist the onset of hydroelastic instabilities. It was also shown that, generally, the smaller the hydraulic diameter, the less stable the system, because of the increased virtual mass.

It should be noted that no great importance should be attached to the numerical values in the above calculations. The same phenomena occur at different values of the parameters for different physical systems. Calculations for twelve-bundle strings (N=12) showed that similar phenomena occur in this case also.

5.3 Convergence to the continuously flexible system

It is noted that the general character of the free motions is similar to that of a single cantilevered cylinder in axial flow [2], [5]. It is reasonable to expect that for $k_0=\infty$, $c_i=\infty$, $k_i=0$, i=1, 2,...N, as N increases the articulated system should converge to the continuously flexible one of [2]. A set of calculations were conducted for a horizontal string involving "bundles" of a single cylinder and constant properties, for the sake of simplicity. The parameters used were $(L/D_i)C_f=\pi/4$, $D_i/D_h=0$, $D_{eq}=D_i$, $k_0=\infty$, $1/c_i=k_i=0$ for i=1,2,...N; L is the overall length, and $\ell_1=\ell_2=\ldots=\ell_{N-1}=\ell$, $\ell_N=\frac{1}{2}\ell$.

The results for the lowest two eigenfrequencies are shown in Fig. 7(a) and 7(b). In Fig. 7(a), the dimensionless flow velocity $u=(M_i/EI)^{\frac{1}{2}}UL=1$ for the continuous system and $u=(M_iLN/k_i^*)^{\frac{1}{2}}U=1$ for the articulated one, and f=0.8 and $C_b=0.05\pi$. In Fig. 7(b) f=1 and $C_b=0$; in this case the system is buckled in the first mode so that the frequency is purely imaginary.

We note that in both cases the convergence is quite good in the first and second modes if N>8.

6. Conclusion

This simple one-dimensional mathematical model for fuel string dynamics must be regarded as the most elementary possible for describing the fluid-elastic behaviour of what is a quite complex structure. Work is continuing with the aim of improving the model, and extending it to yield the response to a prescribed force field.

Of course, like all such models, its success must be assessed by comparing its predictions to experimental results. Work along these lines has already begun [6], by testing the theory of Ref. [2] upon which the present model largely relies, involving continuously flexible as opposed to articulated systems in confined flows; indeed, the work of §5.3 shows the pertinence of such an experimental program for the problem at hand.

Already, the model has been used in connection with the CANDU-BLW fuel design, and it has yielded useful information in assessing its dynamical performance and by showing possible ways for improving its dynamical behaviour in flow, if improvement should be deemed necessary. Conversely, some possible, and plausible, design changes were proven inadvisable, as they may result in hydroelastic instabilities not present in the current design.

Even if this mathematical model proves incapable of giving precise quantitative information on the flow-induced vibration of fuel strings, but gives good qualitative information, its usefulness would be great in permitting one to conduct computer experiments (as opposed to real full scale experiments) as a means to effecting design changes and improving performance.

7. Acknowledgements

This work is the result of a wider scope co-operative effort in the field of nuclear fuel dynamics between Atomic Energy of Canada Ltd. and McGill University. The author would like to express his thanks to AECL, and particularly to M.J. Pettigrew of the Chalk River Nuclear Laboratories who was in charge of the supporting work on this topic undertaken by AECL; also, to L. Kates and E. Reimer of CRNL who developed the matrix operator techniques, described as the "second method" in §3. I would also like to thank N. Chepurniy of McGill University for writing the FORMAC programs associated with the "first method" of §3.

The author also acknowledges the support given to the more fundamental aspects of this research by the National Research Council of Canada.

References

[1] PAÏDOUSSIS, M.P. "The Dynamical Behaviour of Cylindrical Structures in Axial Flow", *Annals of Nuclear Science and Engineering*, 1, 83-106 (1974).

[2] PAÏDOUSSIS, M.P. "Dynamics of Cylindrical Structures Subjected to Axial Flow", *J. Sound Vib.*, 29, 365-385 (1973).

[3] TRUFYN, N. "*A Guide to FORMAC*", Inst. Computer Science, University of Toronto; Toronto, Ont., Canada (1970).

[4] CARLUCCI, L.N. and FORREST, C.F. "*Vibration of Top and Bottom Supported 18-element Fuel Strings in Cold Water Upflow*", CWAPD-249, Canadian Westinghouse (Aug. 1972).

[5] PAÏDOUSSIS, M.P. "Dynamics of Flexible Slender Cylinders in Axial Flow; Part 1. Theory", *J. Fluid Mech.*, 26, 717-736 (1966).

[6] PETTIGREW, M.J. and PAÏDOUSSIS, M.P. "Dynamics and Stability of Flexible Cylinders Subjected to Liquid and Two-Phase Axial Flow in Confined Annuli", Paper D2/6 to be presented in 3rd S.M.i.R.T. Conference, London (1975).

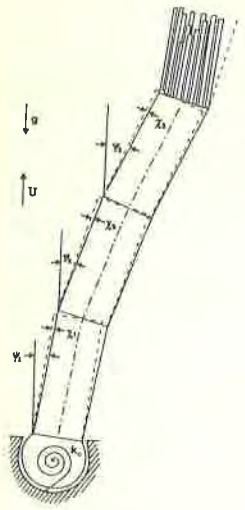

Fig. 1. Schematic diagram of fuel string showing kinematics of deformation. (Note that $\phi_i=\psi_1+\chi_i$.)

```
TH(2,2,1) = C(2) + KCST(2) + KCST(1) + OODH(L2)*CF(12)*D(12)*SN*RH
1O(12)*L(2)*L(2)*U(12)**2*(1.000/2.0D0) + A(12)*RHO(12)*G*L(2)*L(1
22) + A(12)*RHO(L(2)*L(2)*L(12)*UP(12)*U(12) + A(10)*RHO(10)*G*L(2)*
3L(10) + A(10)*RHO(10)*U(10)*UP(10)*L(2)*L(10) + RHO(11)*D(11)*CF(1
41)*OODH(11)*SN*L(2)*U(11)**2*L(11)*(1.0D0/2.0D0) + RHO(11)*C(11)*C
5F(11)*SN*L(2)*U(11)**2*L(11)*(1.0D0/2.0D0) + RHO(11)*A(11)*G*L(2)*
6L(11) + RHO(11)*A(11)*UP(11)*L(2)*U(11)*L(11) + CF(12)*D(12)*SN*RH
7O(12)*L(2)*L(12)*U(12)**2*(1.0D0/2.0D0) + RHO(9)*D(9)*CF(9)*OODH(9
A)*SN*U(9)**2*L(2)*L(9)*(1.0D0/2.0D0) + RHO(9)*D(9)*CF(9)*SN*U(9)**
92*L(2)*L(9)*0.5D0
TH(2,2,1)= TH(2,7,1)          + RHO(9)*A(9)*G*L(2)*L(9) + RHO(9)*A(9)*
AUP(9)*U(9)*L(2)*L(9) + RHO(10)*D(10)*CF(10)*OODH(10)*SN*U(10)**2*L
B(2)*L(10)*(1.0D0/2.0D0) + RHO(10)*D(10)*CF(10)*SN*U(10)**2*L(2)*L(
C10)*(1.0D0/2.0D0) + RHO(7)*OODH(7)*D(7)*CF(7)*SN*L(7)**2*L(2)*L(7)
D*(1.0D0/2.0D0) + RHO(7)*A(7)*G*L(2)*L(7) + RHO(7)*A(7)*UP(7)*U(7)*
EL(2)*L(7) + RHO(7)*D(7)*CF(7)*SN*L(7)**2*L(2)*L(7)*(1.0D0/2.0D0) +
F CF(5)*RHO(8)*L(8)*OODH(9)*SN*U(8)**2*L(2)*L(8)*(1.0D0/2.0D0) + CF
G(8)*RHO(8)*D(8)*SN*U(8)**2*L(2)*L(8)*(1.0D0/2.0D0) + RHO(8)*A(8)*G
H*L(2)*L(8) + RHO(8)*A(8)*U(8)*UP(8)*L(2)*L(8) + A(5)*RHO(5)*G*L(2)
I*L(5) + A(5)*RHO(5)*UP(5)*U(5)*L(2)*L(5)
TH(2,2,1)=TH(2,2,1)                + RHO(6)*D(6)*CF(6)*OODH(
J6)*SN*U(6)**2*L(2)*L(6)*(1.0D0/2.0D0) + RHO(6)*D(6)*CF(6)*SN*U(6)*
K*2*L(2)*L(6)*(1.0D0/2.0D0) + RHO(6)*A(6)*G*L(2)*L(6) + RHO(6)*A(6)
L*U(6)*UP(6)*L(2)*L(6) + RHO(4)*D(4)*CF(4)*OODH(4)*SN*U(4)**2*L(2)*
ML(4)*(1.0D0/2.0D0) + RHO(4)*D(4)*CF(4)*SN*U(6)**2*L(2)*L(4)*(1.0D0
*/2.0D0) + RHO(4)*A(4)*G*L(2)*L(4) + RHO(4)*A(4)*UP(4)*U(4)*L(2)*L(
C4) + RHO(5)*D(5)*CF(5)*OODH(5)*SN*U(5)**2*L(2)*L(5)*(1.0D0/2.0D0)
D+ RHO(5)*D(5)*CF(5)*SN*U(5)**2*L(2)*L(5)*(1.0D0/2.0D0) + RHO(2)*OO
EDH(2)*D(2)*CF(2)*SN*L(2)**2*L(2)**2*(1.0D0/4.0D0) + RHO(2)*A(2)*G*
RL(2)**2*(1.0D0/2.0D0) + RHO(2)*A(2)*U(2)*UP(2)*L(2)**2*(1.0D0/2.0D
5O) + RHO(2)*D(2)*CF(2)*SN*U(2)**2*L(2)**2*(1.0D0/4.0D0) + CF(1)*RH
TO(1)*D(1)*OODH(1)*SN*U(1)**2*L(1)*(1.0D0/2.0D0) + CF(1)*RHO(1)
U*D(1)*SN*U(1)**2*L(1)*L(2)*(1.0D0/2.0D0) + RHO(1)*A(1)*G*L(1)*L(2
V) + RHO(1)*A(1)*UP(1)*U(1)*L(2) + RHO(12)*DEO**2*CB*L(2)*L(12)*
W*OO(12)*D(1)*(1.0D0/2.0D0) + RHO(12)*DEO**2*CP*L(2)*L(12)**2*UP(
X12)*2*(1.0D0/2.0D0)
TH(2,2,1)=TH(2,2,1) + RHO(12)*DEO**2*CA*L(2)*U(12)**2*(1.0D0/2.0E
Y0)-G*SM(3)*L(3)*L(2)-G*SM(2)*L(2)**2*(1.0D0/2.0D0)-G*SM(5)*L(2)*L(
Z5)-G*SM(4)*L(2)*L(4)-G*SM(6)=L(2)*L(6)-G*SM(9)*L(2)*L(9)-G*SM(8)*L
1(2)*L(8)-G*SM(7)*L(2)*L(7)-G*SM(11)*L(2)*L(11)-G*SM(10)*L(2)*L(10)
2-G*L(2)*SM(2)*L(12)-RM(2)*U(2)**2*L(2)-RM(2)*UP(2)**2*L(2)**3*(1.
3000/12.000)
```

Fig. 2. Excerpt of the FORMAC computer print-out giving the coefficient of $\ddot{\phi}_2$ in the second equation of motion, denoted by TH(2,2,1), in the case of N=12. (In this case $\rho'=0$, $M'=0$).

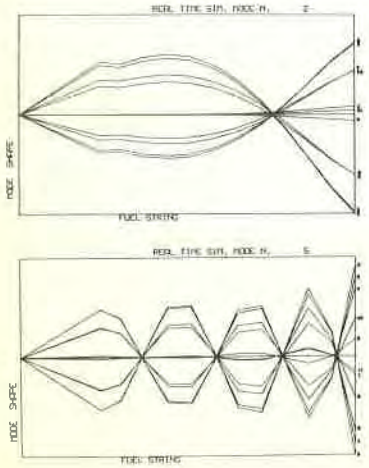

Fig. 3. The modal shapes of the second and fifth modes of a typical case for N=12, with flow present.

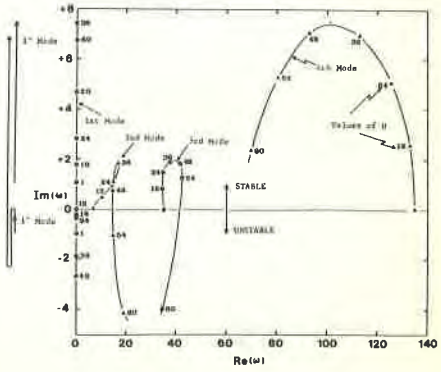

Fig. 4. Eigenfrequencies of a typical N=4 system, plotted as an Argand diagram, as functions of U.

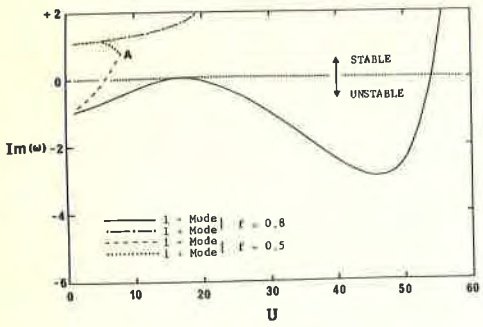

Fig. 5. The two branches of the first mode [Re(ω)=0], showing the effect of streamlining of the free end

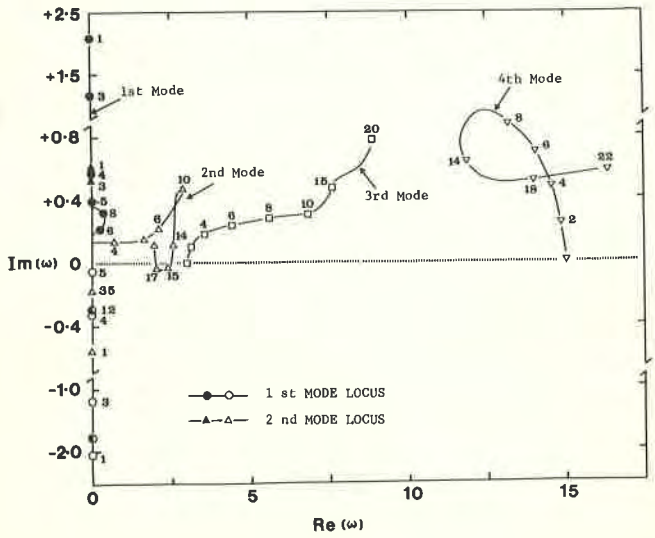

Fig. 6. The eigenfrequencies of the system of Fig. 4, but with the stiffnesses ten times less and the lengths doubled.

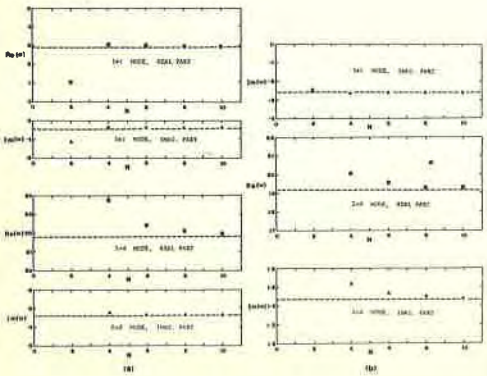

Fig. 7. Convergence of the eigenfrequencies to continuous case for a typical cantilevered system. (a) with f=0.8, u=1, and (b) with f=1, u=3. ---, continuous system; ▲,●, articulated system.